catalysts

MDPI

Article

Microstructural Changes in $La_{0.5}Ca_{0.5}Mn_{0.5}Fe_{0.5}O_3$ Solid Solutions under the Influence of Catalytic Reaction of Methane Combustion

Evgeny Yu. Gerasimov [1,2,*], Vladimir A. Rogov [1,2], Igor P. Prosvirin [1], Lyubov A. Isupova [1] and Sergey V. Tsybulya [1,2]

[1] Boreskov Institute of Catalysis SB RAS, 630090 Novosibirsk, Russia; rogov@catalysis.ru (V.A.R.); prosvirin@catalysis.ru (I.P.P.); isupova@catalysis.ru (L.A.I.); tsybulya@catalysis.ru (S.V.T.)

[2] Novosibirsk National Research University, 630090 Novosibirsk, Russia

* Correspondence: gerasimov@catalysis.ru; Tel.: +73-833-269-534

Received: 29 April 2019; Accepted: 20 June 2019; Published: 24 June 2019

Abstract: This article attempts to study changes in the microstructure of solid solutions with the perovskite structure $La_{0.5}Ca_{0.5}Mn_{0.5}Fe_{0.5}O_3$ under the action of the methane oxidation reaction medium. By the methods of XRD, XPS and HRTEM the initial condition of the structure and the surface of the perovskite were both investigated. A feature of the structure of this solid solution is the presence of planar defects in the direction of the planes (101). After the methane oxidation reaction, a similar study of perovskite structure was conducted to obtain the changes. It was shown that under the action of the reaction medium, $Ca_{1-x}Mn_xO$ particles form on the surface of the perovskite phase, while planar defects in $La_{0.5}Ca_{0.5}Mn_{0.5}Fe_{0.5}O_3$ structure remain. In situ XRD experiments on perovskite calcination in helium current up to 750 °C showed the formation of a similar $Ca_{1-x}Mn_xO$ phase on the perovskite surface.

Keywords: perovskite; catalytic oxidation of methane; planar defects; solid solutions; in situ XRD

1. Introduction

Solid solutions with perovskite structure have been intensively studied in recent decades due to a wide and unique set of their physical and chemical properties [1–5]. Certain properties, such as the effect of colossal magnetic resistance, charge ordering, magnetic calorimetric effect [6–9] are not a complete list found in the perovskite structure. The effects are caused by quite labile structure of the parent compound with the general formula ABO_3. In real crystals, positions A and B can be occupied by different ions, including dissimilar ones, which can lead to the formation of cation-deficient structures [10,11]. For example, materials based on $La_{1-x}M_xMeO_3$ (M = Ca, Sr, Ba, Me = Mn, Fe, Co) at high temperatures have mixed ionic and electronic conductivity and can be used in high-temperature electrochemical devices such as gas sensors, oxygen permeable membranes and electrodes of solid-state fuel cells and catalysts of high-temperature oxidizing processes [12–14].

Catalytic oxidation of methane has been the subject of numerous publications in recent decades [15]. Perovskites are used as catalysts in the reaction of partial oxidation of methane [16–18] and as a deep methane oxidation catalysts [19–21]. The main task of which was to obtain chemical compositions with the highest possible activity at the lowest possible temperatures. From the literature data [22–25] it is known that the most active were supported palladium catalysts, which provided a high degree of CH_4 oxidation already at 300–450 °C. However, metal oxide-supported PdO catalysts tend to deactivate below 450 °C, which seriously hinders their long-term application in catalytic combustion. Later it was shown that at higher temperatures (up to 550–650 °C) compounds with perovskite structure (ABO_3)

including oxides of rare-earth metals and 3D elements can compete with Pd-supported catalysts [26,27]. Such compounds are more preferable due to their higher thermal stability and the high cost of noble metals.

A significant aspect in the creation of functional materials is the choice of the method of synthesis and subsequent modification treatments that can lead to the formation of an optimal structure, from the point of view of catalytic properties [28,29]. An important aspect in solving the problems of creating materials based on the perovskite structure used at high temperatures is the reversible nature of oxygen loss and addition during heating/cooling of these oxides [20,30]. One of the ways to solve this problem is the introduction of doping elements to improve the transport properties of solid solutions with perovskite structure. The introduction of bivalent cations to the perovskite A-sublattice containing, as a rule, trivalent cations contributes to the formation of cation vacancies positively affecting the transport of oxygen in the perovskite structure. Simultaneous introduction of variable valency cations such as Mn, Fe, Co to the B-sublattice of the perovskite phase also improves the transport properties of oxygen from the catalyst volume to the surface [31].

Solid solutions ($LaMn_{1-x}Fe_xO_3$) can also be used as active and stable catalysts for complete oxidation in gas purification processes [32,33], The introduction of Ca^{2+} cations into the La sublattice increases the mobility of O^{2-} anions in the system [34], which positively affects the catalytic activity of samples in deep oxidation reactions, but reduces their thermal and structural stability in media with a low oxygen content. The introduction of Mn cations into the iron sublattice, on the contrary, can contribute to the stabilization of the perovskite structure at high temperatures, preventing the formation of vacancy-ordered phases.

In this study, we investigated the preparation and characterization of $La_{0.5}Ca_{0.5}Mn_{0.5}Fe_{0.5}O_3$ perovskite catalyst by Pechini method and its application to methane combustion. Additional studies of the effect of the reaction medium on the microstructure of perovskite were carried out using the TEM, XPS and XRD methods.

2. Results and Discussion

2.1. Catalyst Characterization

According to ICP MS data obtained on the device Agilent 7700 (USA), the initial compound has a total composition of $La_{0.52}Ca_{0.48}Mn_{0.50}Fe_{0.50}O_{3-\delta}$, which was close to the given chemical formula. The values obtained are presented in Table 1. Measurement of the specific surface area by thermal desorption of argon showed a surface value of 9.3 m^2/g, which is the average value for perovskites synthesized by Pechini method (from polymer–salt compositions) at temperatures of 900 °C [35].

Table 1. ICP MS data $La_{0.5}Ca_{0.5}Mn_{0.5}Fe_{0.5}O_3$.

Sample Name/Mass %	La	Ca	Mn	Fe
$La_{0.5}Ca_{0.5}Mn_{0.5}Fe_{0.5}O_3$	32.8	8.7	13.8	14.2

According to XRD pattern (Figure 1) $La_{0.5}Ca_{0.5}Mn_{0.5}Fe_{0.5}O_3$ is a well-crystallized solid solution with a perovskite structure (PDF Number: 70-2665) having orthorhombic modification (space group Pnma), which corresponds to the data obtained in Reference [36] for $CaLaMnFeO_6$ and for $La_{0.6}Ca_{0.4}Mn_{1-x}Fe_xO_3$ [37] structures. Reflexes characteristic to the presence of other phases on the XRD pattern were not found. The unit cell parameters were calculated using Rietveld refinement procedure and gave values: a = 5.429 (6) Å, b = 7.671 (6) Å, c = 5.472 (4) Å. The volume of the unit cell of $La_{0.5}Ca_{0.5}Mn_{0.5}Fe_{0.5}O_3$ was V = 227.9 $Å^3$. The coherent scattering region calculated by the Selyakov–Scherrer formula was 260 Å.

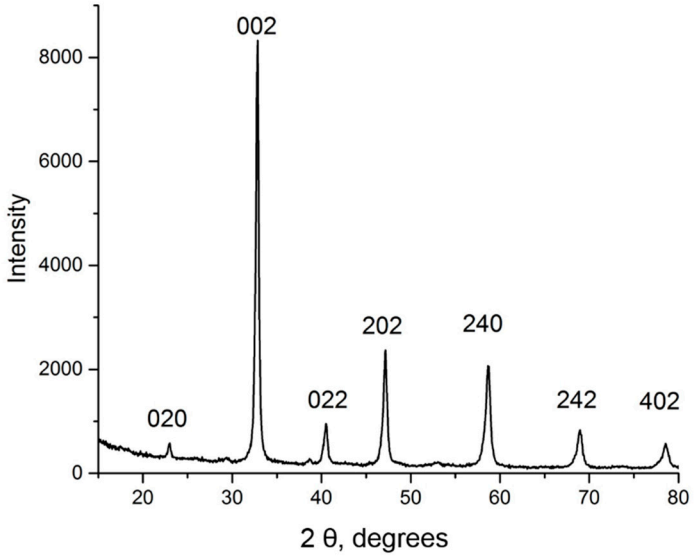

Figure 1. XRD pattern of the fresh $La_{0.5}Ca_{0.5}Mn_{0.5}Fe_{0.5}O_3$ with orthorhombic indexes.

According to HRTEM images, $La_{0.5}Ca_{0.5}Mn_{0.5}Fe_{0.5}O_3$ consists of rounded lamellar particles with an average diameter of about 30 nm (consistent with the coherent scattering region calculated from the XRD data). Particles form agglomerates with sizes from 20 nm to several microns (Figure 2a). A distinctive feature of these particles is the presence of planar defects observed in the form of contrast lines (marked with white arrows), randomly located on the surface of the particles. At higher magnifications, it can be seen that the defects are located in the planes (101). This type of defects in the structure of the perovskite $La_{1-x}Ca_xFeO_3$ was observed in [38], where the composition of the perovskite included Fe cations in the initial state and in the perovskites $La_{1-x}Ca_xMnO_3$ after the oxidation reaction of CH_4 in the sublattice of manganese cations [34]. It is also worth noting the presence of a layer of amorphized carbon on the surface of perovskite particles, the thickness of such a layer is about 0.5 nm.

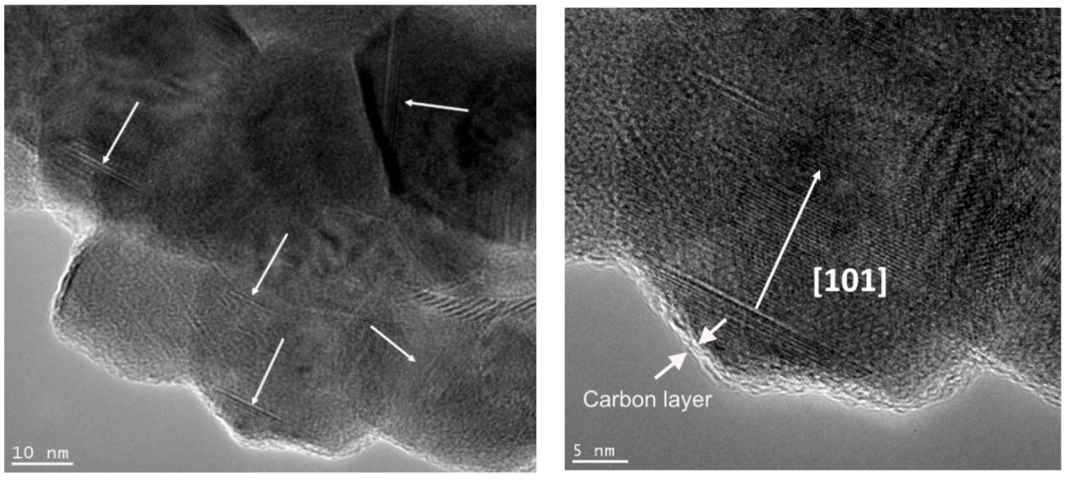

(**a**) (**b**)

Figure 2. HRTEM images of perovskite particles with planar defects (**a**) and crystal lattice of perovskite containing defects in the direction of the planes (101) (**b**).

Analysis of the review photoelectron spectra of the samples showed that only lanthanum, calcium, manganese, iron, carbon and oxygen are present in the samples (Figure 3). No other additional impurities were found within the sensitivity of the XPS method. Analysis of the photoelectron spectra of the Fe2p level of the measured samples allows us to conclude that in the initial samples iron is mainly in the state of Fe^{3+}; this is evidenced by both the value of the binding energy (E = 710.8 ± 0.1 eV) and

the shape of the spectrum line. It is known that in the spectra of Fe^{2+} there are pronounced shake-up satellites located approximately 6 eV higher in the binding energy from the main lines. In the spectra of Fe^{3+}, shake-up satellites are also observed, which are much weaker in intensity, but shifted to a greater value of the binding energy from the main peak of iron (~8 eV). This situation is observed in the Fe2p spectra of the studied samples. From the analysis of Mn 2p level photoelectron spectra, it can be concluded that there is a superposition of peaks from the two states of manganese. In the initial sample, manganese is mainly in the Mn^{3+} state, in addition, the small shoulder is observed from the large values of the binding energy 642.3 ± 0.1 eV. This value is typical for Mn^{4+}. The ratio of Mn^{4+} to Mn^{3+} is 0.94, which practically corresponds to the degree of doping with calcium cations.

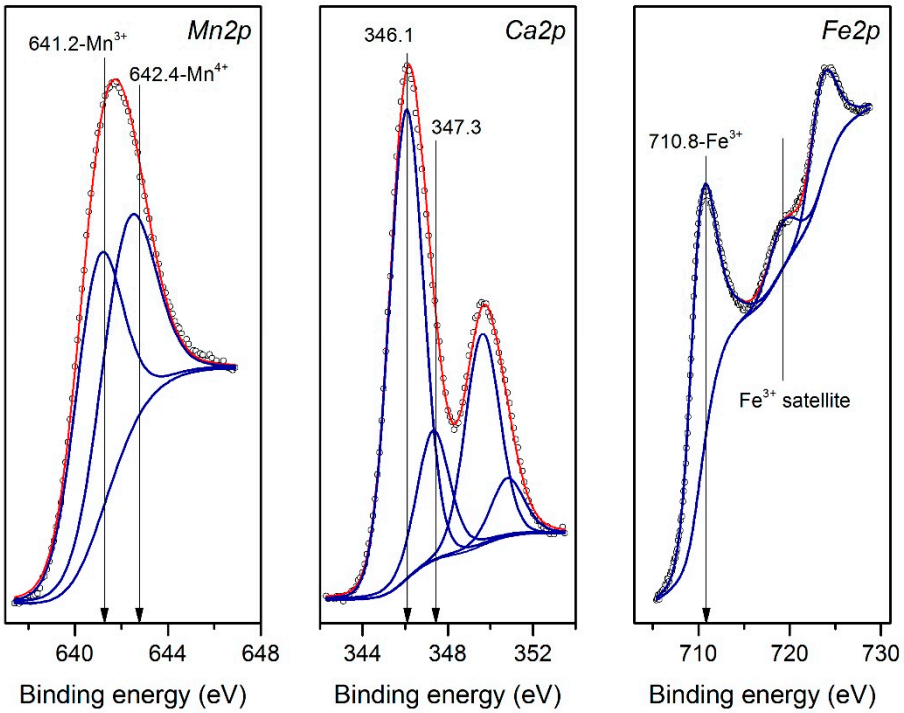

Figure 3. XPS spectra of the fresh sample $La_{0.5}Ca_{0.5}Mn_{0.5}Fe_{0.5}O_3$ with line deconvolution.

2.2. $La_{0.5}Ca_{0.5}Mn_{0.5}Fe_{0.5}O_3$ Catalytic Activity and Microstructure Modifications in the Methane Combustion Reaction

The data of catalytic activity of the sample are given in Table 2. In the temperature range up to 400 °C, the catalytic activity is not significant. At 400 °C activity is about 25%, with an increase in temperature up to 450 °C and 500 °C, significant increase in conversion up to 93.7% occurs. With an increase in temperature to 600 °C, methane conversion is 100% while only products of complete oxidation (CO_2 and H_2O) are formed. After reducing the temperature to 500 °C, the conversion slightly reduces, but remains almost at the same level with the previous value.

Table 2. $La_{0.5}Ca_{0.5}Mn_{0.5}Fe_{0.5}O_3$ dependence of methane conversion on temperature of reaction medium.

Temperature, °C	CH_4 Conversion, %
400	25.46
450	60.71
500	93.72
550	99.52
600	100
500	90.02

The study of the solid solution after catalytic tests by XRD (Figure 4) revealed no significant changes in the structure of the sample. There was a slight increase in the volume of the unit cell. It can be seen by slightly shift of spent catalyst XRD pattern to small angle region.

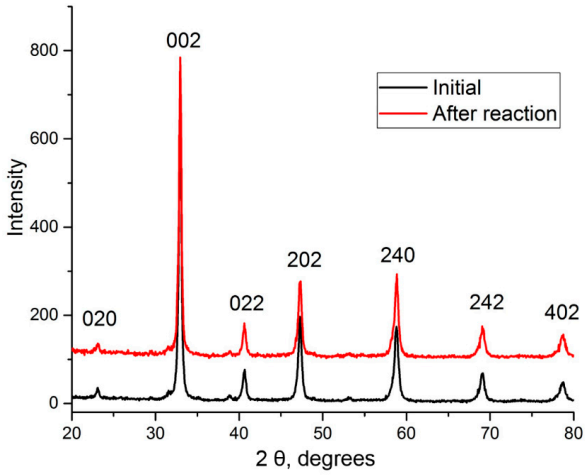

Figure 4. XRD patterns of the fresh (black line) and spent (red line) $La_{0.5}Ca_{0.5}Mn_{0.5}Fe_{0.5}O_3$.

However, the study sample by the method of HRTEM showed the presence of CaO particles on the surface of the perovskite phase. In this case, planar defects in the direction of the planes (101) were preserved (Figure 5a). The number of these defects is small, since no superstructural peaks were found in the initial sample and in the sample after catalytic tests according to XRD data. XRD method has also not recorded the allocation of CaO phase. Measurement of the interplanar spacings of the Ca-containing particles on the surface of the perovskite phases showed smaller values of interplanar spacings (2.68 Å) than in CaO structure (2.77 Å for (111) spacing). It can be concluded that the particles also include the cations of Mn (Figure 5b), i.e., it is a solid solution $Ca_{1-x}Mn_xO$ having a crystal structure similar to CaO. In [39] the authors conducted similar studies on the calcination of solid solutions $La_{1-x}Ca_xMnO_3$, the separation of CaO and Mn_3O_4 phases on the surface of perovskite particles was observed. Apparently, the formation of a solid solution occurs due to the simultaneous presence of Mn, Ca and Fe cations in the perovskite structure. Examples of the formation of such solid solutions are given in Reference [40], however, its formation on the surface of perovskite, according to available literature data, the authors observe for the first time.

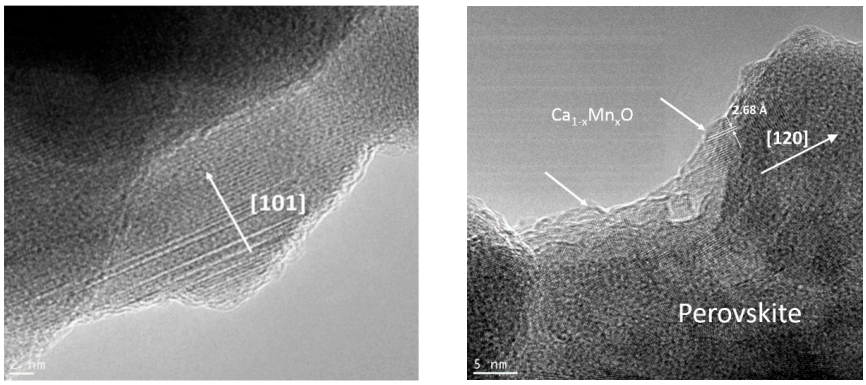

(**a**) (**b**)

Figure 5. HRTEM images of perovskite particle after participation in methane oxidation reaction with planar defects (**a**) and $Ca_{1-x}Mn_xO$ aggregates on the perovskite surface (**b**).

It is possible that the appearance of Ca-Mn-O particles on the surface of the perovskite phase is due to the lower oxygen content in the gas phase. Moreover, the reduction of the sample is the cause of the observed slight decrease in catalytic activity during the catalytic tests.

Indeed, according to TPR-H_2 (Figure 6) in the sample after catalytic tests, the total hydrogen absorption is significantly reduced (in 5.6 times), mainly due to a decrease in the absorption at low (400 °C and 600 °C) temperatures, which indicates a sufficiently strong reduction of the sample during the test. The amount of hydrogen absorbed by the sample decreases after catalytic tests—from 2.73×10^{-3} to 0.49×10^{-3} mol H_2/g. In addition, the profile of the recovery curve also varies significantly, which indicates a change in the structure of the near-surface layers of the catalyst as a result of the reaction. According to the data given in Reference [41], the main peak observed in the temperature range of 400–500 °C refers to the recovery of high-charged Mn^{4+} and Mn^{3+} cations to the Mn^{2+} state, the peaks in the region of 600 °C can be attributed to the recovery of iron +3 to +2 cations. The high-temperature region of 800 °C refers to the recovery of iron cations almost to the metal state [42].

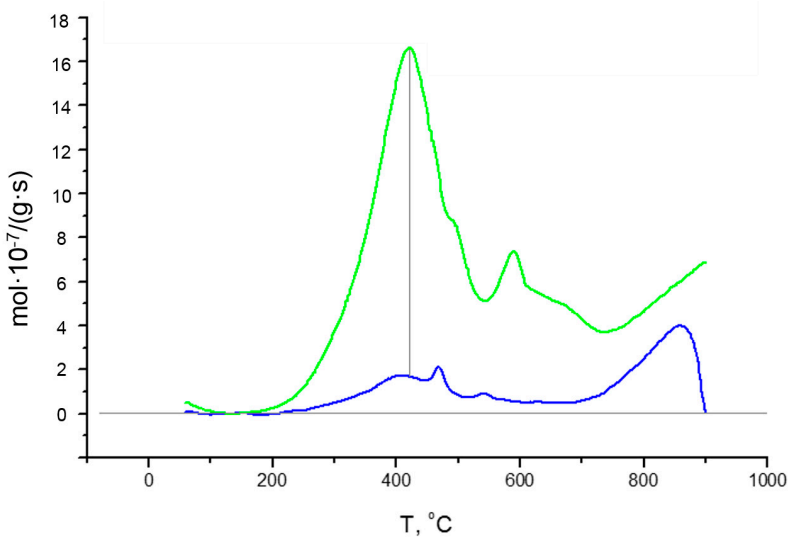

Figure 6. TPR-H_2 profiles of the $La_{0.5}Ca_{0.5}Mn_{0.5}Fe_{0.5}O_3$ before (green line) and after (blue line) methane combustion reaction.

2.3. Formation Process of the Ca-Mn-O Phase on the Surface of the Perovskite in He Atmosphere

For a more detailed study of the catalyst reduction processes, in situ XRD experiments were carried out on heating of the catalyst in the helium current to a temperature of 750 °C, which was slightly higher than the temperature of the methane oxidation reaction. XRD patterns obtained during the study are shown in Figure 7. In the range of 300–600 °C the perovskite structure has not undergone significant changes. XRD patterns demonstrated only peak displacements associated with thermal expansion. However, at a temperature of 750 °C peaks characteristic for the $Ca_{1-x}Mn_xO$ were observed on XRD pattern. The unit cell volume increased with temperature rising. Cooled to room temperature, the unit cell parameters did not return to the original state (Table 3). This fact can be associated with the formation of vacancies in the structure of perovskite occurred as a result of the allocation of Mn and Ca cations at the $La_{0.5}Ca_{0.5}Mn_{0.5}Fe_{0.5}O_3$ surface.

According to photoelectron spectra of the Ca2p region (Figure 8) of the studied samples after testing in helium flow up to 750 °C, it can be concluded that in the spectra two main peaks with binding energies of 346.2 ± 0.1 and 347.1 ± 0.2 eV are observed. The first value is characteristic of calcium in the composition of perovskite, and the peak with a large binding energy can be attributed to $Ca_{1-x}Mn_xO$.

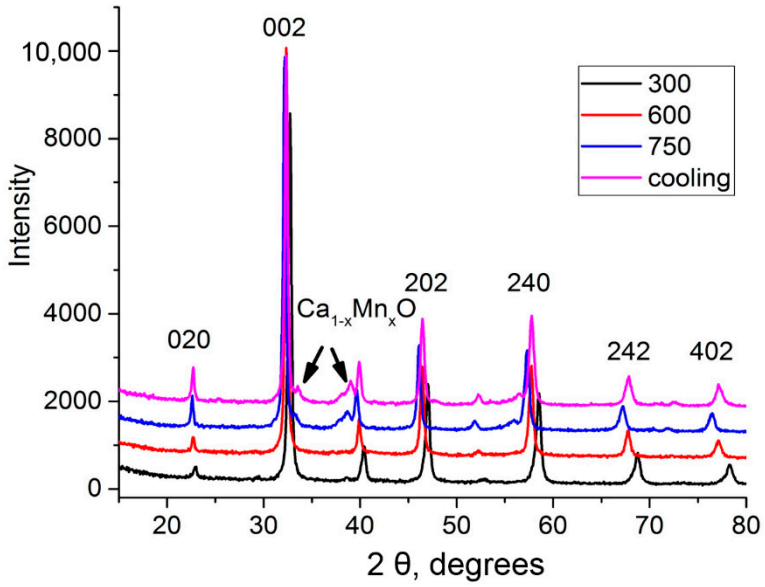

Figure 7. In situ XRD patterns of $La_{0.5}Ca_{0.5}Mn_{0.5}Fe_{0.5}O_3$ in He flow heating. Magenta line is cooling to room temperature.

Table 3. Unit cell parameters for the $La_{0.5}Ca_{0.5}Mn_{0.5}Fe_{0.5}O_3$ in He flow heating.

Temperature, °C	a, Å	b, Å	c, Å	V, Å^3
30	5.43	7.67	5.47	227.92
300	5.46	7.71	5.47	230.51
600	5.53	7.83	5.54	239.66
750	5.57	7.87	5.57	244.18
cooling	5.53	7.81	5.54	238.72

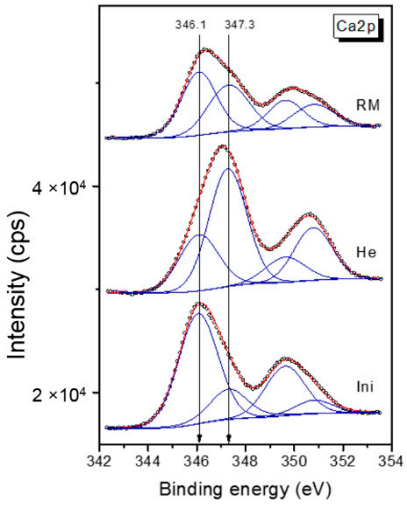

Figure 8. Ca2p level spectra of the studied samples.

The XPS data confirm the formation of $Ca_{1-x}Mn_xO$ on the surface of the perovskite phase, the proportion of Ca cations on the surface increases significantly both as a result of the participation of the catalyst in the reaction and after calcination of the sample in the He current (Table 4). At the same time, the amount of Mn cations in the calcined in He flow sample is higher than after reaction, which can indicate the formation of a larger number of the $Ca_{1-x}Mn_xO$ phase on the surface of $La_{0.5}Ca_{0.5}Mn_{0.5}Fe_{0.5}O_3$.

Table 4. The ratio of atomic concentrations of the elements presented in the studied samples.

Samples	Mn/Fe	Fe/La	Mn/La	Mn/Ca	Fe/Ca	La/Ca
Initial	1.15	0.69	0.80	0.36	0.31	0.45
He treatment	1.16	0.61	0.70	0.21	0.18	0.30
After reaction	0.97	0.76	0.73	0.26	0.27	0.35

According to TGA (Figure 9) sample lost about 3.8% of the mass when heated in He up to 1000 °C. In the temperature range from 30° to 300 °C the sample lost 2.1% of the mass, which can be associated with the removal of water, CO, –OH groups and adsorbed oxygen from the surface of the sample. Further heating of the sample up to 300 °C–600 °C led to removing of the weakly bound lattice oxygen, which was 0.9%. At the next stage (600°–800 °C), the sample lost about 0.7% of its mass. A wide exothermic peak accompanied this change in mass on the DTA curve at 700 °C. It corresponds to the data obtained from the experiment in situ XRD and is evidence of the formation of a massive phase $Ca_{1-x}Mn_xO$. At higher temperatures, the TGA curve showed a slight decrease in the mass about 0.1%.

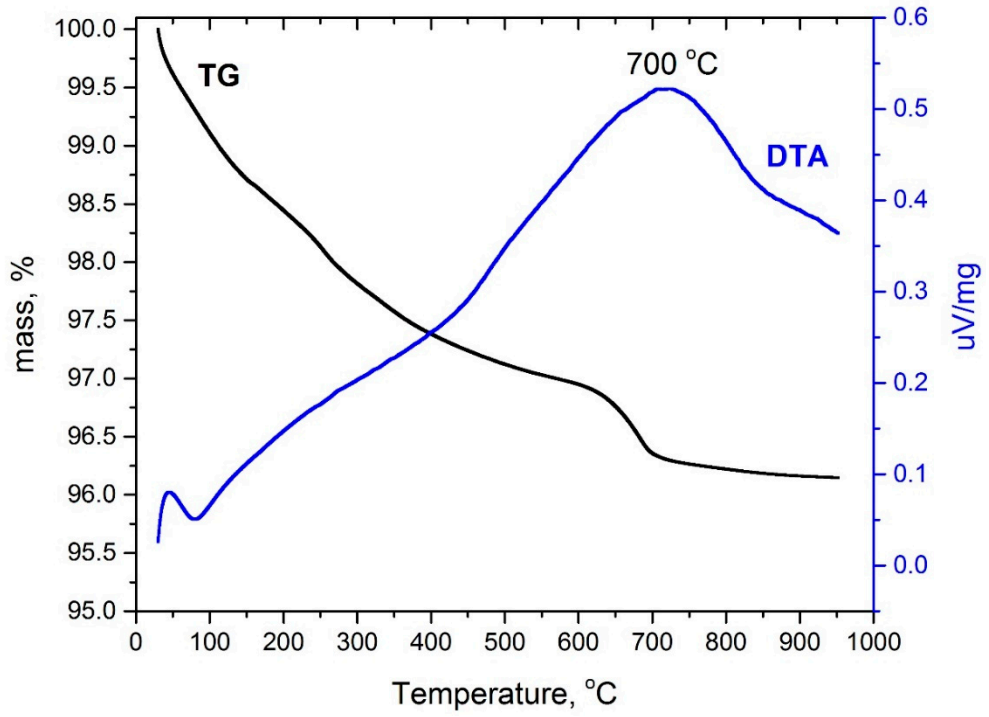

Figure 9. Thermoanalytical data obtained in the heating of $La_{0.5}Ca_{0.5}Mn_{0.5}Fe_{0.5}O_3$ in He flow.

3. Materials and Methods

$La_{0.5}Ca_{0.5}Mn_{0.5}Fe_{0.5}O_3$ sample was synthesized by the polymerizable precursor (Pechini) method. For this purpose, appropriate amounts of aqueous solutions of lanthanum, calcium, manganese and iron nitrates were combined, citric acid and ethylene glycol were added, and the mixture was evaporated at 70–80 °C until the formation of a resinous polymer (polymer–salt stock). The polymer was subjected to oxidative destruction. The precursor was calcined at 900 °C for four hours with a rise in temperature of 100 °C/h.

The catalytic activity of the samples in a reaction of methane oxidation was determined in a flow system at temperatures of 350–600 °C. A 1-g portion of a catalyst fraction of 0.25–0.5 mm was mixed with 1 cm^3 of quartz and placed in a U-shaped quartz reactor with an inside diameter of 4.5 mm. The feed rate of a reaction mixture of 0.9% CH_4 + 9% O_2 (and the balance N_2) was 2.4 L/h. Before the measurements, the sample was kept in the reaction mixture for ~30 min at a specified temperature. After testing at 600 °C, the sample was cooled in the reaction mixture to 500 °C and its activity was

determined once again. Only carbon dioxide and water were the oxidation products of methane. The reaction products were determined by chromatography.

Electron microscopy investigation (HRTEM) was performed using a JEM-2200FS (JEOL Ltd., Tokyo, Japan) electron microscope operated at 200 kV with a lattice resolution 0.1 nm for obtaining HRTEM images.

XRD patterns were obtained on the Bruker AXS D8 Advance diffractometer (Karlsruhe, Germany) equipped with a high-temperature and supplying of various gas mixtures and the use of CuKα radiation on scanning with a step of 2θ = 0.05° point by point and an accumulation time of 3 s at each point in a range of the angles 2θ = 15°–80°. Each temperature measurement was performed according to the following conditions: temperature rate of 5 °C/min with He flow of 40 mL/min. Before the measurements, the sample was kept for ~30–50 min at a specified temperature. XRD patterns were processed using X'Pert High Plus software (PANanalytical B.V. Almelo, Netherlands).

XPS (X-Ray Photoelectron Spectroscopy) data were obtained on the SPECS photoelectron spectrometer (Berlin, Germany) using non-monochromatized MgK* radiation (h* = 1253.6 eV, 150 W). The binding energy scale was pre-calibrated to the position of the core level peaks Au 4f7/2 (84.0 eV) and Cu2p3/2 (932.67 eV). The sample was applied to a double-sided conductive adhesive tape. The effect of recharging, arising in the process of electron photoemission, was taken into account by the method of internal standard, as used C1s carbon line (284.8 eV), which is part of hydrocarbon inclusions [43]. Determination of the relative content of elements on the surface of catalysts and the ratio of atomic concentrations was carried out by the integrated intensities of photoelectron lines corrected for the corresponding atomic sensitivity coefficients: C1s—1.0, Ca2p—5.13, O1s—2.85, Mn2p3/2—8.99, Fe2p—16.0, La3d5/2—26.5.

The TPR study of samples with hydrogen were performed in a flow system with a thermal-conductivity detector (LHM-8, LHM, Yoshkar-Ola, USSR) using a fraction of samples with a particle size of 0.25–0.5 mm. Before the reduction, the samples were pretreated in argon at 150 °C for 0.5 h and cooled to room temperature. The samples weight were 75 mg; the flow rate of the reducing mixture (10% H_2 in Ar) was 40 mL/min. The samples were heated at a rate of 10 °C/min to 900 °C. The hydrogen uptake (in $mol \cdot g^{-1} \cdot s^{-1}$) was calculated from calibration obtained for the reduction of standardized sample of copper oxide (CuO). The peak areas of the TPR of samples corresponding to hydrogen consumption (mmoL/(g sample)) were calculated with the use of an asymmetric Gaussian function profile.

Thermal analysis of the sample was performed using a synchronous thermal analysis device STA 449C Jupiter company NETZSCH (Germany). This device combines the methods of differential thermal analysis (DTA) and thermogravimetry analysis (TGA) in one dimension. The weight of the sample was approximately 100 mg. The furnace temperature was increased from 40 °C to 980 °C at a rate of 10 °C/min with He flux of 30 mL/min. The sample weight was monitored continuously as a function of temperature.

4. Conclusions

The solid solution $La_{0.5}Ca_{0.5}Mn_{0.5}Fe_{0.5}O_3$ with orthorhombic perovskite structure was synthesized by the method of polymer–salt compositions. A distinctive feature of this solid solution is the presence of planar defects in the particles in the direction of the crystallographic planes (101).

The catalytic activity study of perovskite in the methane oxidation reaction in the temperature range of 300–600 °C showed that already at 400 °C 25% of methane conversion was achieved, and at a temperature of 550 °C was almost 100%, while only products of complete oxidation (CO_2 and H_2O) were formed. The study by HRTEM showed the formation of $Ca_{1-x}Mn_xO$ particles with sizes of about 10 nm on the surface of perovskite after reaction. According to XRD data, the formation of these particles after methane oxidation reaction was not detected, which indicated a small amount of oxide.

According to the XRD and TG data, $Ca_{1-x}Mn_xO$ phase formation on the perovskite surface occurs at a temperature of 700 °C in helium flow. The impact of the environment with low oxygen

content leads to an increase in the proportion of calcium cations on the surface of the solid solution. The formation of $Ca_{1-x}Mn_xO$ is not typical for perovskites $La_{1-x}Ca_xMnO_3$, and occurs due to the simultaneous presence of Fe and Mn cations in one perovskite sublattice.

Author Contributions: E.Y.G., L.A.I. and S.V.T. planned and designed the experiments. I.P.P. performed the catalyst characterization by X.P.S. E.Y.G. performed the characterization by T.E.M. and X.R.D. V.A.R. performed TPR-H_2 tests. L.A.I. performed the catalytic activity tests. E.Y.G. wrote the manuscript. L.A.I. and S.V.T. revised the manuscript. All authors discussed the results and approved the final version of the manuscript.

Funding: This work was supported by the Russian Science Foundation, grant № 18-73-00139.

Conflicts of Interest: The authors declare no conflict of interest.

References

1. Zhu, J.; Li, H.; Zhong, L.; Xiao, P.; Xu, X.; Yang, X.; Zhao, Z.; Li, J. Perovskite oxides: Preparation, characterizations, and applications in heterogeneous catalysis. *ACS Catal.* **2014**, *4*, 2917–2940. [CrossRef]
2. Najjar, H.; Batis, H. Development of Mn-based perovskite materials: Chemical structure and applications. *Catal. Rev.* **2016**, *58*, 371–438. [CrossRef]
3. Keav, S.; Matam, S.; Ferri, D.; Weidenkaff, A.; Keav, S.; Matam, S.K.; Ferri, D.; Weidenkaff, A. Structured Perovskite-Based Catalysts and Their Application as Three-Way Catalytic Converters—A Review. *Catalysts* **2014**, *4*, 226–255. [CrossRef]
4. Niu, G.; Guo, X.; Wang, L. Review of recent progress in chemical stability of perovskite solar cells. *J. Mater. Chem. A* **2015**, *3*, 8970–8980. [CrossRef]
5. Wu, H.; Li, L.; Liang, L.-Z.; Liang, S.; Zhu, Y.-Y.; Zhu, X.-H. Recent progress on the structural characterizations of domain structures in ferroic and multiferroic perovskite oxides: A review. *J. Eur. Ceram. Soc.* **2015**, *35*, 411–441. [CrossRef]
6. Dong, Q.Y.; Zhang, H.W.; Sun, J.R.; Shen, B.G.; Franco, V. A phenomenological fitting curve for the magnetocaloric effect of materials with a second-order phase transition. *J. Appl. Phys.* **2008**, *103*, 116101. [CrossRef]
7. Izyumov, Y.A.; Skryabin, Y.N. Double exchange model and the unique properties of the manganites. *Uspekhi Fiz. Nauk* **2001**, *171*, 121.
8. Haghiri-Gosnet, A.-M.; Renard, J.-P. CMR manganites: Physics, thin films and devices. *J. Phys. D Appl. Phys.* **2003**, *36*, R127–R150. [CrossRef]
9. Granger, P.; Parvulescu, V.I.; Kaliaguine, S.; Prellier, W. *Perovskites and Related Mixed Oxides: Concepts and Applications*; John Wiley & Sons: Hoboken, NJ, USA, 2015; ISBN 9783527686605.
10. Takacs, M.; Hoes, M.; Caduff, M.; Cooper, T.; Scheffe, J.R.; Steinfeld, A. Oxygen nonstoichiometry, defect equilibria, and thermodynamic characterization of LaMnO3 perovskites with Ca/Sr A-site and Al B-site doping. *Acta Mater.* **2016**, *103*, 700–710.
11. Elsiddig, Z.A.; Xu, H.; Wang, D.; Zhang, W.; Guo, X.; Zhang, Y.; Sun, Z.; Chen, J. Modulating Mn 4+ Ions and Oxygen Vacancies in Nonstoichiometric LaMnO 3 Perovskite by a Facile Sol-Gel Method as High-Performance Supercapacitor Electrodes. *Electrochim. Acta* **2017**, *253*, 422–429.
12. Malkhandi, S.; Yang, B.; Manohar, A.K.; Manivannan, A.; Prakash, G.K.S.; Narayanan, S.R. Electrocatalytic Properties of Nanocrystalline Calcium-Doped Lanthanum Cobalt Oxide for Bifunctional Oxygen Electrodes. *J. Phys. Chem. Lett.* **2012**, *3*, 967–972. [CrossRef] [PubMed]
13. Kucharczyk, B.; Okal, J.; Tylus, W.; Winiarski, J.; Szczygieł, B. The effect of the calcination temperature of LaFeO3 precursors on the properties and catalytic activity of perovskite in methane oxidation. *Ceram. Int.* **2019**, *45*, 2779–2788. [CrossRef]
14. Mueller, D.N.; Machala, M.L.; Bluhm, H.; Chueh, W.C. Redox activity of surface oxygen anions in oxygen-deficient perovskite oxides during electrochemical reactions. *Nat. Commun.* **2015**, *6*, 6097. [CrossRef] [PubMed]
15. Wang, W.; Yuan, F.; Niu, X.; Zhu, Y. Preparation of Pd supported on La(Sr)-Mn-O Perovskite by microwave Irradiation Method and Its Catalytic Performances for the Methane Combustion. *Sci. Rep.* **2016**, *6*, 19511. [CrossRef] [PubMed]

16. De Santana Santos, M.; Neto, R.C.R.; Noronha, F.B.; Bargiela, P.; da Rocha, M.D.G.C.; Resini, C.; Brandão, S.T. Perovskite as catalyst precursors in the partial oxidation of methane: The effect of cobalt, nickel and pretreatment. *Catal. Today* **2018**, *299*, 229–241.
17. Roseno, K.T.C.; Brackmann, R.; da Silva, M.A.; Schmal, M. Investigation of LaCoO3, LaFeO3 and LaCo0.5Fe0.5O3 perovskites as catalyst precursors for syngas production by partial oxidation of methane. *Int. J. Hydrogen Energy* **2016**, *41*, 18178–18192. [CrossRef]
18. De, K.T.; Schmal, M.; Brackmann, R.; Alves, R.M.B.; Giudici, R. Partial oxidation of methane on neodymium and lanthanium chromate based perovskites for hydrogen production. *Int. J. Hydrogen Energy* **2019**, *44*, 8166–8177.
19. Alifanti, M.; Auer, R.; Kirchnerova, J.; Thyrion, F.; Grange, P.; Delmon, B. Activity in methane combustion and sensitivity to sulfur poisoning of La1−xCexMn1−yCoyO3 perovskite oxides. *Appl. Catal. B Environ.* **2003**, *41*, 71–81. [CrossRef]
20. Marchetti, L.; Forni, L. Catalytic combustion of methane over perovskites. *Appl. Catal. B Environ.* **1998**, *15*, 179–187. [CrossRef]
21. Szabo, V.; Bassir, M.; Van Neste, A.; Kaliaguine, S. Perovskite-type oxides synthesized by reactive grinding: Part IV. Catalytic properties of LaCo1−xFexO3 in methane oxidation. *Appl. Catal. B Environ.* **2003**, *43*, 81–92.
22. Banerjee, A.; McGuire, J.; Lawnick, O.; Bozack, M. Low-Temperature Activity and PdO-PdOx Transition in Methane Combustion by a PdO-PdOx/γ-Al2O3 Catalyst. *Catalysts* **2018**, *8*, 266. [CrossRef]
23. Schwartz, W.R.; Pfefferle, L.D. Combustion of Methane over Palladium-Based Catalysts: Support Interactions. *J. Phys. Chem. C* **2012**, *116*, 8571–8578. [CrossRef]
24. Bassil, J.; AlBarazi, A.; Boutros, M. Catalytic combustion of methane over mesoporous silica supported palladium. *Catal. Today* **2011**, *176*, 36–40. [CrossRef]
25. Choudhary, T.; Banerjee, S.; Choudhary, V. Catalysts for combustion of methane and lower alkanes. *Appl. Catal. A Gen.* **2002**, *234*, 1–23. [CrossRef]
26. Yang, J.; Guo, Y. Nanostructured perovskite oxides as promising substitutes of noble metals catalysts for catalytic combustion of methane. *Chin. Chem. Lett.* **2018**, *29*, 252–260. [CrossRef]
27. Royer, S.; Duprez, D.; Can, F.; Courtois, X.; Batiot-Dupeyrat, C.; Laassiri, S.; Alamdari, H. Perovskites as Substitutes of Noble Metals for Heterogeneous Catalysis: Dream or Reality. *Chem. Rev.* **2014**, *114*, 10292–10368. [CrossRef] [PubMed]
28. Melo Jorge, M.; Correia dos Santos, A.; Nunes, M. Effects of synthesis method on stoichiometry, structure and electrical conductivity of CaMnO3−δ. *Int. J. Inorg. Mater.* **2001**, *3*, 915–921. [CrossRef]
29. Tan, L.; Gu, X.; Yang, L.; Jin, W.; Zhang, L.; Xu, N. Influence of powder synthesis methods on microstructure and oxygen permeation performance of Ba0.5Sr0.5Co0.8Fe0.2O3−δ perovskite-type membranes. *J. Membr. Sci.* **2003**, *212*, 157–165. [CrossRef]
30. Leontiou, A.; Ladavos, A.; Bakas, T.; Vaimakis, T.; Pomonis, P. Reverse uptake of oxygen from La1−xSrx (Fe3+/Fe4+)O3±δ perovskite-type mixed oxides (x = 0.00, 0.15, 0.30, 0.40, 0.60, 0.70, 0.80, 0.90). *Appl. Catal. A Gen.* **2003**, *241*, 143–154. [CrossRef]
31. Ponce, S.; Peña, M.; Fierro, J.L. Surface properties and catalytic performance in methane combustion of Sr-substituted lanthanum manganites. *Appl. Catal. B Environ.* **2000**, *24*, 193–205. [CrossRef]
32. Zhao, K.; He, F.; Huang, Z.; Wei, G.; Zheng, A.; Li, H.; Zhao, Z. Perovskite-type LaFe1−x MnxO3 (x=0, 0.3, 0.5, 0.7, 1.0) oxygen carriers for chemical-looping steam methane reforming: Oxidation activity and resistance to carbon formation. *Korean J. Chem. Eng.* **2017**, *34*, 1651–1660. [CrossRef]
33. Zheng, S.; Hua, Q.; Gu, W.; Liu, B. Catalytic oxidation of CO on LaMn1−xFexO3 perovskites solid solution. *J. Mol. Catal. A Chem.* **2014**, *391*, 7–11. [CrossRef]
34. Isupova, L.A.; Gerasimov, E.Y.; Zaikovskii, V.I.; Tsybulya, S.V.; Kulikovskaya, N.A.; Saputina, N.F. Synthesis of homogeneous La1–xCaxMnO3 solid solutions by the Pechini method and their activity in methane oxidation. *Kinet. Catal.* **2009**, *50*, 886–891. [CrossRef]
35. Isupova, L.A.; Kulikovskaya, N.A.; Saputina, N.F.; Gerasimov, E.Y.; Tsybulya, S.V. La1-xCaxFeO3-δ (x = 0-1) perovskites prepared by the Pechini method: Catalytic activity in deep methane and CO oxidation. *Kinet. Catal.* **2015**, *56*, 781–787. [CrossRef]
36. Shaheen, R.; Bashir, J.; Rundlöf, H.; Rennie, A.R. The crystal structure of CaLaMnFeO6 double perovskite. *Mater. Lett.* **2005**, *59*, 2296–2299. [CrossRef]

37. Othmani, S.; Balli, M.; Cheikhrouhou, A. Structural, magnetic and magnetocaloric properties of La0.6Ca0.4Mn1−xFexO3 (x=0, 0.05, 0.1, 0.15 and 0.2) manganites. *Solid State Commun.* **2014**, *192*, 51–55. [CrossRef]
38. Gerasimov, E.Y.; Isupova, L.A.; Tsybulya, S.V. Microstructural features of the La1−xCaxFeO3−δ solid solutions prepared via Pechini route. *Mater. Res. Bull.* **2015**, *70*, 291–295. [CrossRef]
39. Isupova, L.A.; Gerasimov, E.Y.; Zaikovskii, V.I.; Tsybulya, S.V. Effect of the reaction medium on the structure of the La1−xCaxMnO3 (x = 0–1) solid solutions prepared by the pechini method. *Kinet. Catal.* **2011**, *52*, 104–110. [CrossRef]
40. Jay, A.H.; Andrews, K.W. Note on oxide systems pertaining to steel - making furnace slags: FeO-MnO, FeO-MgO, CaO-MnO, MgO-MnO. *J. Iron Steel Inst.* **1946**, *152*, 15–18.
41. Yakovleva, I.S.; Isupova, L.A.; Rogov, V.A.; Sadykov, V.A. Forms of oxygen in La1−xCaxMnO3 + δ (x = 0–1) perovskites and their reactivities in oxidation reactions. *Kinet. Catal.* **2008**, *49*, 261–270. [CrossRef]
42. Isupova, L.A.; Yakovleva, I.S.; Rogov, V.A.; Alikina, G.M.; Sadykov, V.A. Oxygen States in Oxides with a Perovskite Structure and Their Catalytic Activity in Complete Oxidation Reactions: System $La_{1-x}Ca_xFeO_{3-y}$ (x = 0–1). *Kinet. Catal.* **2004**, *45*, 446–453. [CrossRef]
43. Moulder, J.F.; Stickle, W.F.; Sobol, P.E.; Bomben, K.D. *Handbook of X-ray Photoelectron Spectroscopy*; Chastain, J., Ed.; Perkin-Elmer: Eden Prairie, MN, USA, 1992.